

# Time-step dependent force interpolation scheme for suppressing numerical Cherenkov instability in relativistic particle-in-cell simulations

Yingchao Lu<sup>a,b</sup>, Patrick Kilian<sup>a</sup>, Fan Guo<sup>a</sup>, Hui Li<sup>a</sup>, Edison Liang<sup>b</sup>

<sup>a</sup>Theoretical Division, Los Alamos National Laboratory, Los Alamos, New Mexico, 87545, USA

<sup>b</sup>Department of Physics and Astronomy, Rice University, Houston, Texas 77005, USA

---

## Abstract

The WT scheme, a piecewise polynomial force interpolation scheme with time-step dependency, is proposed in this paper for relativistic particle-in-cell (PIC) simulations. The WT scheme removes the lowest order numerical Cherenkov instability (NCI) growth rate for arbitrary time steps allowed by the Courant condition. While NCI from higher order resonances is still present, the numerical tests show that for smaller time steps, the numerical instability grows much slower than using the optimal time step found in previous studies. The WT scheme is efficient for improving the quality and flexibility of relativistic particle-in-cell simulations.

*Keywords:* Particle-in-cell, Numerical Cherenkov instability, Plasma

---

## 1. Introduction

The particle-in-cell (PIC) method[1] is widely used for the simulations of plasma dynamics ranging from Laser Plasma Accelerators (LPAs) to collisionless astrophysical problems. In the PIC method, quasi-particles are used to sample the distribution of physical charged particles in phase space. The equations of motion of quasi-particles are solved using a particle-push algorithm, e.g. Boris algorithm[1]. The electromagnetic field is defined on a grid, usually the staggered Yee grid[2]. The Lorentz force acting on a quasi-particle is calculated by interpolating the electromagnetic field from nearby grid points to the quasi-particle location using a force interpolation scheme. The on-grid current density is calculated using a current deposition scheme according to the quasi-particle motion and is used to update the on-grid electromagnetic field. The PIC method can be implemented without solving a Poisson equation for the electric potential if one use an exact charge conservation scheme. Although the exact charge conservation current deposition scheme[3] allows an arbitrary form-factor for quasi-particle, the most commonly used form-factor is a B-spline function. Using B-splines has a few advantages[4], including the easiness of computation due to their polynomial nature, the smoothness of the charge assigned to the grid as the particle moves across the grid, and the negligible fluctuations at long-range. If one requires momentum to be conserved, then the force interpolation function should be identical to the charge assignment function. Higher order B-spline functions have better smoothness and long-range properties, but are more computationally expensive.

Relativistic PIC simulations with drifting plasma beams are vulnerable to an electromagnetic numerical instability know as the Numerical Cherenkov instability (NCI)[5]. This numerical instability is caused by the resonance between two modes in the numerical method: (1) the vacuum electromagnetic mode, which has a deviation of the dispersion relation from the physical one, i.e.  $\omega = ck$ , due to the discretization of Maxwell equations, (2) the drifting plasma beam mode, which is dispersionless but has it's aliasing beam modes[6]. This resonance is a numerical artifact and unphysical. It is desirable to have an efficient numerical method which significantly suppress the NCI in order to improve the quality of relativistic PIC simulations. An analytical expression for lowest order NCI growth rate was derived[7]. The numerically most unstable mode and it's growth rate can be calculated from the analytical expression without carrying out any numerical experiments. It was found that in the momentum conserving scheme, if one uses time step  $\Delta t = \frac{\Delta x_1}{2c}$  for a drifting plasma in  $x_1$  direction where  $\Delta x_1$  is the grid spacing in  $x_1$  direction, the lowest order NCI growth rate vanishes[8].

In this work, we propose a time-step dependent force interpolation scheme which removes the lowest order NCI growth for a drifting plasma in  $x_1$  direction for arbitrary time step allowed by the Courant condition, not just for  $\Delta t = \frac{\Delta x_1}{2c}$ . We call this interpolation scheme the “WT scheme”, which stands for “weighting with time-step dependency”, or for the form of multidimensional interpolation function having

---

*Email address:* yclu@lanl.gov (Yingchao Lu)

$W$ 's and  $T$ 's as in Eq(16). The quasi-particle form-factor for charge assignment is still a B-spline function and the electrostatic part of the self-force vanishes for the WT scheme. The WT scheme recovers the momentum conserving scheme[9, 10] for the case where the time step is  $\Delta t = \frac{\Delta x_1}{2c}$  and the grid spacings in all directions are the same. In the WT scheme, the lowest order NCI growth rate still vanishes if the spatial derivative stencil in the Faraday equation are modified[11] while keeping the spatial derivative stencil in the Ampere equation. However, the asymptotic expression for NCI growth rate only shows the lowest order growth rate. High order terms do contribute to the actually numerical simulations, but are complicated to derive analytically. On the other hand, the numerical instabilities evolve nonlinearly after saturation in the actually simulations. Thus numerical experiments are carried out to quantify the behavior of NCI in full PIC simulations. The numerical tests show that the simulation using the WT scheme is more numerically stable if the time step is reduced. The WT scheme has little impact on the computational cost, and thus is potentially more efficient compared to the spatial Fourier transform based methods, such as Pseudo-Spectral Time Domain(PSTD) algorithms[12] for which the lowest order NCI resonance is removed by improving the phase velocity of the electromagnetic wave.

This paper is organized as follows. In Sec 2, we derive the expression for WT scheme. In Sec 3, we describe a few additional considerations for relativistic PIC method. The results for numerical experiments is given in Sec 4.

## 2. WT scheme

For a three-dimensional electromagnetic PIC code with momentum conserving (MC)[9, 10] and exact charge conservation scheme[3] in Cartesian coordinate, the electromagnetic field that is spatially interpolated from grid point  $\mathbf{x}_g = (x_{g,1}, x_{g,2}, x_{g,3}) = (n_1\Delta x_1, n_2\Delta x_2, n_3\Delta x_3)$  ( $n_1, n_2, n_3$  can be half-integer or integer depending whether the component of electromagnetic field has a half-grid offset in the  $i$ -th direction) to a particle position  $\mathbf{x} = (x_1, x_2, x_3)$  can be expressed as

$$E_i(\mathbf{x}) = \sum_{n_1, n_2, n_3} W_l(\mathbf{x} - \mathbf{x}_g) E_i(\mathbf{x}_g) \quad B_i(\mathbf{x}) = \sum_{n_1, n_2, n_3} W_l(\mathbf{x} - \mathbf{x}_g) B_i(\mathbf{x}_g) \quad (1)$$

and the on-grid charge density of a quasi-particle is calculated from the form-factor

$$\rho(\mathbf{x}_g) = \frac{q}{V_c} W_l(\mathbf{x} - \mathbf{x}_g) \quad (2)$$

where

$$W_l(\mathbf{x} - \mathbf{x}_g) = W_l^{(1)}(x_1 - x_{g,1}) W_l^{(2)}(x_2 - x_{g,2}) W_l^{(3)}(x_3 - x_{g,3}) \quad (3)$$

and  $W_l^{(i)}$  is the  $l$ -th order B-spline with width  $(l+1)\Delta x_i$  in  $i$ -th direction, and  $V_c$  is the volume of a mesh cell, for one-dimensional schemes,  $V_c = \Delta x_1$ , for two dimensions,  $V_c = \Delta x_1 \Delta x_2$  and for three,  $V_c = \Delta x_1 \Delta x_2 \Delta x_3$ . In the exact charge conservation scheme[3], the current density associated with the motion of a single quasi-particle is the unique linear combination of form-factor differences in consistency with the discrete continuity equation. The Fourier transformation of the interpolation tensor in Eq(1) is[7]

$$\begin{aligned} S_{E1} &= s_{l,1} s_{l,2} s_{l,3} \eta_1 & S_{B1} &= \cos(\omega' \Delta t / 2) s_{l,1} s_{l,2} s_{l,3} \eta_2 \eta_3 \\ S_{E2} &= s_{l,1} s_{l,2} s_{l,3} \eta_2 & S_{B2} &= \cos(\omega' \Delta t / 2) s_{l,1} s_{l,2} s_{l,3} \eta_1 \eta_3 \\ S_{E3} &= s_{l,1} s_{l,2} s_{l,3} \eta_3 & S_{B3} &= \cos(\omega' \Delta t / 2) s_{l,1} s_{l,2} s_{l,3} \eta_1 \eta_2 \end{aligned} \quad (4)$$

where the factor  $\eta_i = (-1)^{\nu_i}$  is multiplied when the electromagnetic field has a half-grid offset in the  $i$ -th direction, and

$$s_{l,i} = \left( \frac{\sin(k'_i \Delta x_i / 2)}{k'_i \Delta x_i / 2} \right)^{l+1} \quad (5)$$

and the aliasing frequency and wave vectors with aliasing order  $(\mu, \nu_1, \nu_2, \nu_3)$  are

$$\omega' = \omega + \mu \frac{2\pi}{\Delta t}, \quad \mu = 0, \pm 1, \pm 2, \dots \quad k'_i = k_i + \nu_i \frac{2\pi}{\Delta x_i}, \quad \nu_i = 0, \pm 1, \pm 2, \dots \quad (6)$$

There is one momentum conserving interpolation tensor for each  $l$ , and we call it  $MCl$ .

Derived in Ref. [7], the asymptotic expression for NCI growth rate for a cold drifting plasma beam traveling in  $x_1$  direction with an ultra-relativistic speed  $v_1 \rightarrow c$  is

$$\Gamma = \frac{\sqrt{3}}{2} \left| \frac{\omega_p^2 c^2 S_{J1} \{ (S_{B3} \xi_0 - S_{E2} [k]_{B1c}) [k]_{E2} k_2 + (S_{B2} \xi_0 - S_{E3} [k]_{B1c}) [k]_{E3} k_3 \}}{2 \xi_0^2 \xi_1} \right|^{1/3} \quad (7)$$

where  $S_{J_i}$  is the interpolation tensor for the current density after Fourier transformation[7], and  $\omega_p = \sqrt{\frac{4\pi q^2 n_e}{\gamma_0 m_e}}$  is the relativistic plasma frequency, and the bulk Lorentz factor is  $\gamma_0 = \frac{1}{\sqrt{1-\beta^2}} = \frac{1}{\sqrt{1-v_1^2/c^2}}$ , and the finite difference operators are

$$[\omega] = \frac{\sin(\omega\Delta t/2)}{\Delta t/2}, \quad [k]_{Ei} = A_i \frac{\sin(k_i\Delta x_i/2)}{\Delta x_i/2}, \quad [k]_{Bi} = \frac{\sin(k_i\Delta x_i/2)}{\Delta x_i/2} \quad (8)$$

where  $[k]_{Ei}$  or  $A_i$  depends on the spatial derivative stencil in Faraday's equation, and  $[k]_{Bi}$  is related to the spatial derivative stencil in Ampere's equation which is unmodified from the standard Yee scheme, and

$$\xi_0 = \frac{\sin(k'_1 c\Delta t/2)}{\Delta t/2}, \quad \xi_1 = \cos(k'_1 c\Delta t/2) \quad (9)$$

For MC scheme where  $S_E$  and  $S_B$  are given by Eq(4), the lowest order NCI growth rate given by Eq(7) depends on time step and only vanishes for  $\Delta t = \frac{\Delta x_i}{c}$ . In order to remove the time-step dependency of the NCI growth rate given by Eq(7), we propose the WT scheme, where we modify Eq(4) to the following form

$$\begin{aligned} S_{E1} &= s_{l,1}\tau_{l,2}\tau_{l,3}\eta_1 & S_{B1} &= \cos(\omega'\Delta t/2)\tau_{l,1}s_{l,2}s_{l,3}\eta_2\eta_3 \\ S_{E2} &= \tau_{l,1}s_{l,2}\tau_{l,3}\eta_2 & S_{B2} &= \cos(\omega'\Delta t/2)s_{l,1}\tau_{l,2}s_{l,3}\eta_1\eta_3 \\ S_{E3} &= \tau_{l,1}\tau_{l,2}s_{l,3}\eta_3 & S_{B3} &= \cos(\omega'\Delta t/2)s_{l,1}s_{l,2}\tau_{l,3}\eta_1\eta_2 \end{aligned} \quad (10)$$

where

$$\tau_{l,i} = \left(\frac{\sin(k'_i\Delta x_i/2)}{k'_i\Delta x_i/2}\right)^l \left(\frac{\sin(k'_i c\Delta t)}{k'_i c\Delta t}\right) \quad (11)$$

For the interpolation tensor in Eq(10), the expression for lowest order NCI growth rate vanishes for arbitrary time step  $\Delta t$  as shown in Appendix A. For  $\Delta t = \frac{\Delta x_i}{2c}$ , we have  $\tau_{l,i} = s_{l,i}$ , which recovers the MC scheme.

To get the interpolation function in real space, we calculate the inverse Fourier transform of  $s_{l,i}$  and  $\tau_{l,i}$ . We constrain our discussion to  $\Delta t \leq \frac{\Delta x_i}{2c}$ , because for  $\Delta t > \frac{\Delta x_i}{2c}$  the width of the interpolation function becomes large and more grid points are needed for interpolation. The inverse Fourier transform of  $s_{l,i}$  is simply the  $(l+1)$ -th order B-spline function  $W_l^{(i)}$ . The interpolation function corresponding to  $\tau_{1,i}$  is

$$T_1^{(i)}(\tilde{x}_i) = \mathcal{F}^{-1}(\tau_{1,i}) = \begin{cases} \frac{1+2\Delta\tilde{t}_i-2|\tilde{x}_i|}{4\Delta\tilde{t}_i} & \text{if } \frac{1}{2} - \Delta\tilde{t}_i < |\tilde{x}_i| \leq \frac{1}{2} + \Delta\tilde{t}_i \\ 1 & \text{if } |\tilde{x}_i| \leq \frac{1}{2} - \Delta\tilde{t}_i \\ 0 & \text{otherwise} \end{cases} \quad (12)$$

where  $\mathcal{F}^{-1}$  is the inverse Fourier transform,  $\Delta\tilde{t}_i = \frac{c\Delta t}{\Delta x_i}$ , and  $\tilde{x} = \frac{x_i - x_{g,i}}{\Delta x_i}$  is the normalized coordinate difference between the particle and the grid point. The interpolation function corresponding to  $\tau_{2,i}$  is

$$T_2^{(i)}(\tilde{x}_i) = \mathcal{F}^{-1}(\tau_{2,i}) = \begin{cases} \frac{(\Delta\tilde{t}_i+1-|\tilde{x}_i|)^2}{4\Delta\tilde{t}_i} & \text{if } 1 - \Delta\tilde{t}_i < |\tilde{x}_i| \leq 1 + \Delta\tilde{t}_i \\ 1 - |\tilde{x}_i| & \text{if } \Delta\tilde{t}_i < |\tilde{x}_i| \leq 1 - \Delta\tilde{t}_i \\ \frac{2\Delta\tilde{t}_i - \Delta\tilde{t}_i^2 - \tilde{x}_i^2}{2\Delta\tilde{t}_i} & \text{if } |\tilde{x}_i| \leq \Delta\tilde{t}_i \\ 0 & \text{otherwise} \end{cases} \quad (13)$$

The interpolation function corresponding to  $\tau_{3,i}$  is

$$T_3^{(i)}(\tilde{x}_i) = \mathcal{F}^{-1}(\tau_{3,i}) = \begin{cases} \frac{(3+2\Delta\tilde{t}_i-2|\tilde{x}_i|)^3}{96\Delta\tilde{t}_i} & \text{if } \frac{3}{2} - \Delta\tilde{t}_i < |\tilde{x}_i| \leq \frac{3}{2} + \Delta\tilde{t}_i \\ \frac{4\Delta\tilde{t}_i^2 + 3(3-2|\tilde{x}_i|)^2}{24} & \text{if } \frac{1}{2} + \Delta\tilde{t}_i < |\tilde{x}_i| \leq \frac{3}{2} - \Delta\tilde{t}_i \\ \frac{-8\Delta\tilde{t}_i^3 - 36\Delta\tilde{t}_i^2(1-2|\tilde{x}_i|) - 3(1-2|\tilde{x}_i|)^3 + 6\Delta\tilde{t}_i(15-12|\tilde{x}_i|-4\tilde{x}_i^2)}{96\Delta\tilde{t}_i} & \text{if } \frac{1}{2} - \Delta\tilde{t}_i < |\tilde{x}_i| \leq \frac{1}{2} + \Delta\tilde{t}_i \\ \frac{9-4\Delta\tilde{t}_i^2-12\tilde{x}_i^2}{12} & \text{if } |\tilde{x}_i| \leq \frac{1}{2} - \Delta\tilde{t}_i \\ 0 & \text{otherwise} \end{cases} \quad (14)$$

The interpolation function corresponding to  $\tau_{4,i}$  is

$$T_4^{(i)}(\tilde{x}_i) = \mathcal{F}^{-1}(\tau_{4,i}) = \begin{cases} \frac{(\Delta\tilde{t}_i+2-|\tilde{x}_i|)^4}{48\Delta\tilde{t}_i} & \text{if } 2 - \Delta\tilde{t}_i < |\tilde{x}_i| \leq 2 + \Delta\tilde{t}_i \\ \frac{(2-|\tilde{x}_i|)(2-|\tilde{x}_i|)^2 + \Delta\tilde{t}_i^2}{6} & \text{if } 1 + \Delta\tilde{t}_i < |\tilde{x}_i| \leq 2 - \Delta\tilde{t}_i \\ \frac{-(1-|\tilde{x}_i|)^4 + 2\Delta\tilde{t}_i(6-6|\tilde{x}_i|+|\tilde{x}_i|^3) - 6\Delta\tilde{t}_i^2(1-|\tilde{x}_i|)^2 + 2\Delta\tilde{t}_i^3|\tilde{x}_i| - \Delta\tilde{t}_i^4}{12\Delta\tilde{t}_i} & \text{if } 1 - \Delta\tilde{t}_i < |\tilde{x}_i| \leq 1 + \Delta\tilde{t}_i \\ \frac{4-6\tilde{x}_i^2+3|\tilde{x}_i|^3 - \Delta\tilde{t}_i^2(2-3|\tilde{x}_i|)}{6} & \text{if } \Delta\tilde{t}_i < |\tilde{x}_i| \leq 1 - \Delta\tilde{t}_i \\ \frac{3\tilde{x}_i^4 + \Delta\tilde{t}_i(16-24\tilde{x}_i^2) + 18\Delta\tilde{t}_i^2\tilde{x}_i^2 - 8\Delta\tilde{t}_i^3 + 3\Delta\tilde{t}_i^4}{24\Delta\tilde{t}_i} & \text{if } |\tilde{x}_i| \leq \Delta\tilde{t}_i \\ 0 & \text{otherwise} \end{cases} \quad (15)$$

The width of  $T_l^{(i)}$  is  $l\Delta x_i + 2c\Delta t$ , which decreases as the time step decreases. There is one WT scheme interpolation tensor for each  $l$ , and we call it WTL. The full interpolation form for electromagnetic field in WTL scheme is

$$\begin{aligned}
E_1(\mathbf{x}) &= \sum_{n_1, n_2, n_3} W_l^{(1)}(x_1 - x_{g,1}) T_l^{(2)}(x_2 - x_{g,2}) T_l^{(3)}(x_3 - x_{g,3}) E_1(\mathbf{x}_g) \\
E_2(\mathbf{x}) &= \sum_{n_1, n_2, n_3} T_l^{(1)}(x_1 - x_{g,1}) W_l^{(2)}(x_2 - x_{g,2}) T_l^{(3)}(x_3 - x_{g,3}) E_2(\mathbf{x}_g) \\
E_3(\mathbf{x}) &= \sum_{n_1, n_2, n_3} T_l^{(1)}(x_1 - x_{g,1}) T_l^{(2)}(x_2 - x_{g,2}) W_l^{(3)}(x_3 - x_{g,3}) E_3(\mathbf{x}_g) \\
B_1(\mathbf{x}) &= \sum_{n_1, n_2, n_3} T_l^{(1)}(x_1 - x_{g,1}) W_l^{(2)}(x_2 - x_{g,2}) W_l^{(3)}(x_3 - x_{g,3}) B_1(\mathbf{x}_g) \\
B_2(\mathbf{x}) &= \sum_{n_1, n_2, n_3} W_l^{(1)}(x_1 - x_{g,1}) T_l^{(2)}(x_2 - x_{g,2}) W_l^{(3)}(x_3 - x_{g,3}) B_2(\mathbf{x}_g) \\
B_3(\mathbf{x}) &= \sum_{n_1, n_2, n_3} W_l^{(1)}(x_1 - x_{g,1}) W_l^{(2)}(x_2 - x_{g,2}) T_l^{(3)}(x_3 - x_{g,3}) B_3(\mathbf{x}_g)
\end{aligned} \tag{16}$$

And the on-grid charge density of a quasi-particle in WT scheme is still given by Eq(2), which can be inserted in the derivation of the current deposition in an exact charge conserving scheme[3]. The combination of Eq(2) with Eq(16) has zero self force under certain condition as shown in Appendix B. WT scheme allows flexibility in the choice of the time step, because the asymptotic expression for NCI growth rate vanishes for arbitrary time step  $\Delta t$ , not just for  $\Delta t = \frac{\Delta x_1}{2c}$  as found in previous studies[7, 8].

### 3. Additional considerations

A few additional considerations in relativistic PIC method are discussed in this section.

*Maxwell solvers:* A fully explicit Maxwell solver is usually more efficient than FFT-based or implicit solvers. The fully explicit Maxwell solvers in Ref. [11], which modifies the spatial derivative stencil in Faraday's equation and keeps the spatial derivative stencil in Ampere's equation, are compatible with the charge conserving deposition scheme[3]. By choosing the coefficients for the stencil in Faraday's equation, the dispersion error can be fourth order, i.e.  $\frac{\omega}{ck} = 1 + O(k\Delta x)^4$ , as shown in Appendix C, while generally the dispersion error for most Maxwell solvers is second order, i.e.  $\frac{\omega}{ck} = 1 + O(k\Delta x)^2$ .

*Relativistic pseudo-particle loading:* For loading pseudo-particles with relativistic drifting distribution, a sampling of the distribution function in the co-moving frame is usually performed and transformed into the simulation frame[13]. Taking the volume transform between two frames into account is significant. Failing to do so can cause error in particle loading for relativistic distributions. We write down the method for loading particles with arbitrary boost velocities in Appendix D.

*Ultra-relativistic scaling:* The scaling relations can be used for Lorentz factor scaling of the ultra-relativistic PIC simulations. The simulation results obtained for one value of  $\gamma_0$  can be scaled to get the results for other values of  $\gamma_0$ , as long as  $\gamma_0$  is large and the initial and boundary condition of the dimensionless equations do not depend on  $\gamma_0$ , where  $\gamma_0$  is the characteristic Lorentz factor of the system.

*Partially skipping calculation:* Current deposition and the particle momentum update can be skipped in the unperturbed plasma flow regions where it is known to follow pure drift motion and be absent of instability. If the initial perturbed region is  $\mathcal{A}(t=0) = \{(x, y, z) | (x, y, z) \in \mathcal{A}_0\}$ , then the perturbed region for a later time  $t > 0$  is  $\mathcal{A}(t) = \{(x_t, y_t, z_t) | (x_t - x_0)^2 + (y_t - y_0)^2 + (z_t - z_0)^2 < c^2 t^2, (x_0, y_0, z_0) \in \mathcal{A}_0\}$ . This kind of skipping not only prevents numerical instabilities from growing, but also reduces the computational cost with the aid of dynamical load balancing. For example, in the PIC simulations for relativistic shock[14], the current deposition and the particle momentum update can be skipped in the upstream flow. Alternatively, one can use expanding box in a setup with simple geometry[14].

### 4. Numerical experiments

We carry out two-dimensional numerical experiments using EPOCH 2D[15] with modified force interpolation scheme by authors. We use a pair plasma for simplicity. The spatial coordinates and the time of the simulations are normalized by the relativistic electron plasma frequency  $\omega_{pe} = \sqrt{\frac{4\pi n_e e^2}{\gamma_0 m_e}}$  and the relativistic electron skin depth  $d_e = c/\omega_{pe} = c/\sqrt{\frac{4\pi n_e e^2}{\gamma_0 m_e}}$ , respectively. We simulate an unmagnetized uniform drifting pair plasma, which should have no instabilities physically. The instabilities in the simulations are

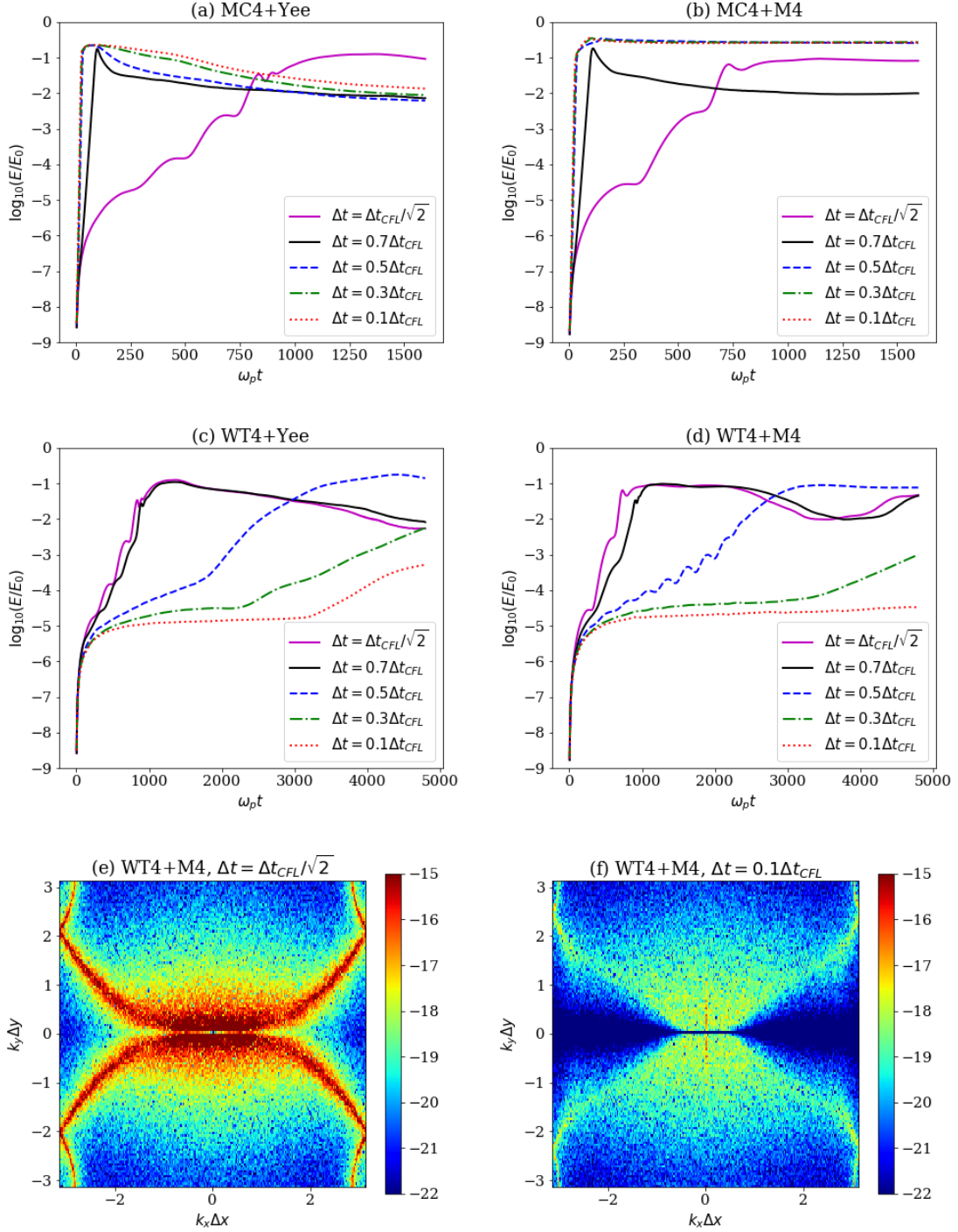


Figure 1: Results for the test problem of drifting pair plasma. (a) The growth history of the fraction of the total electromagnetic energy  $E/E_0$  for MC4 interpolation scheme and Yee solver. (b) Same as (a) but for MC4 interpolation scheme and M4 solver. (c) Same as (a) but for WT4 interpolation scheme and Yee solver. Note that the time axis is different from (a). (d) Same as (a) but for WT4 interpolation scheme and M4 solver. Note that the time axis is different from (a) and (b). (e)  $\log(|\text{FFT}(B_z)|)$  for WT4 scheme and M4 solver, and  $\Delta t = \frac{1}{\sqrt{2}}\Delta t_{CFL}$ . The color bar is the logarithm of field energy in arbitrary units. The simulation time for this frame is  $t = 1080\omega_{pe}^{-1}$ . (f) Same as (a) but with  $\Delta t = 0.1\Delta t_{CFL}$ .

Table 1: Parameters for test problem of drifting pair plasma.

domain size	$L_x = 16d_e, L_y = 8d_e$
boundary condition	Periodic in both $x$ and $y$
number of cells	$N_x = 256, N_y = 128$
pseudo-particles per cell	$N_{\text{PPC}} = 64$ (32 for each species)
drift Lorentz factor	$\gamma = 1000$
temperature	$k_B T_e = k_B T_i = 0.01 m_e c^2$
time step	$\frac{\Delta t}{\Delta t_{\text{CFL}}} = \frac{\Delta t}{\Delta x / (\sqrt{2}c)} = 0.1, 0.3, 0.5, 0.7, \frac{1}{\sqrt{2}}$

always numerical artifacts. The simulations for the unmagnetized uniform drifting pair plasma have been extensively used in literatures[7, 8] for testing NCI in PIC codes. We use the method for loading particles in Appendix D. For the examples we show, we use the WT4 scheme and the regular momentum-conserving MC4 scheme with  $\Delta t \leq \frac{\Delta x}{2c}$  and  $\Delta x_1 = \Delta x_2 = \Delta x$ . For Maxwell solvers, we use the one with fourth order dispersion accuracy (we call it M4), i.e.  $\beta_{12} = \beta_{21} = \delta_1 + \frac{1}{12} = \delta_2 + \frac{1}{12} = \frac{(c\Delta t)^2}{12(\Delta x)^2}$ , as derived in Appendix C and the Yee solver, i.e.  $\beta_{12} = \beta_{21} = \delta_1 = \delta_2 = 0$ . The parameters we use for test problem of a drifting pair plasma are listed in Table 1.

The growth history of the fraction of the total electromagnetic energy  $E/E_0$  is shown in Figure 1(a) to (d), where  $E_0$  is the initial total kinetic energy of all particles and  $E$  is the total energy of electromagnetic field which is a function of time. The growth of  $E/E_0$  is always unphysical after an initial transient that produces electromagnetic fields in thermal equilibrium. In Figure 1(a) where we use MC4 scheme and Yee solver, the case for  $\Delta t = \frac{1}{\sqrt{2}}\Delta t_{\text{CFL}}$  has slower NCI growth than the cases for  $\Delta t \leq 0.7\Delta t_{\text{CFL}}$ , where  $\Delta t_{\text{CFL}} = \frac{\Delta x}{\sqrt{2}c}$ . This is consistent with previous studies[7, 8] and can be explained by the fact that the lowest order NCI growth rate given by Eq(7) vanishes for  $\Delta t = \frac{1}{\sqrt{2}}\Delta t_{\text{CFL}}$  but not for other time steps. In Figure 1(b) where we use M4 solver, the case for  $\Delta t = \frac{1}{\sqrt{2}}\Delta t_{\text{CFL}}$  also has slower NCI growth than other cases, but the time for NCI to saturate is similar to Yee solver. In Figure 1(c) and (d), we use the WT4 scheme. Note that for  $\Delta t = \frac{\Delta t_{\text{CFL}}}{\sqrt{2}}$  the WT scheme recovers the standard momentum conserving scheme, and the scale of time axes for Figure 1(c) and (d) is different from that for Figure 1(a) and (b). In Figure 1(c) where we use WT4 scheme and Yee solver, the NCI grows much slower and saturates at a much later time if a smaller time step is used. For  $\Delta t = 0.3\Delta t_{\text{CFL}}$  and  $\Delta t = 0.1\Delta t_{\text{CFL}}$ ,  $E/E_0$  stays between  $10^{-5}$  to  $10^{-4}$  for a long time. The results for the tests with WT4 scheme and M4 solver is shown in Figure 1(d). In the case for  $\Delta t = 0.3\Delta t_{\text{CFL}}$  and  $\Delta t = 0.1\Delta t_{\text{CFL}}$ , NCI grows slower using M4 solver than using Yee solver. We compare the color coded plots of the logarithm of the out-of-plane magnetic field  $\log(|\text{FFT}(B_z)|)$  as a function of wavenumber, for  $\Delta t = \frac{1}{\sqrt{2}}\Delta t_{\text{CFL}}$  in Figure 1(e), and for  $\Delta t = 0.1\Delta t_{\text{CFL}}$  in Figure 1(f). For both plots we use WT4 scheme and M4 solver. The case for  $\Delta t = 0.1\Delta t_{\text{CFL}}$  has significantly lower numerical instability level than the case for  $\Delta t_{\text{CFL}} = \frac{\Delta x}{\sqrt{2}c}$ .

The trend observed in the numerical tests using WT4 scheme is that NCI grows slower if a smaller  $\Delta t$  is used, which indicates that the high order growth rate which is not included in Eq(7) depends on  $\Delta t$  and decreases as  $\Delta t$  decreases. The detailed analysis of the high order growth rate will be subject of future reports.

## 5. Conclusions

Using the WT scheme, the lowest order NCI growth rate vanishes if the spatial derivative stencil in Ampere's equation is not modified from the standard Yee stencil. The simulation for the drifting pair plasma becomes more numerically stable when decreasing the time step. The WT scheme is efficient for improving the quality and flexibility of relativistic particle-in-cell simulations, although the reason for having small growth rate for small time steps is yet to be understood. The quasi-particle form-factor used for current deposition is unmodified from the standard B-spline function, thus the good smoothness and negligible fluctuations at long-range are retained.

## 6. Acknowledgement

Research presented in this paper was supported by the Center for Space and Earth Science (CSES) program and Laboratory Directed Research and Development (LDRD) program 20200367ER of Los Alamos National Laboratory (LANL). The simulations were performed with LANL Institutional Computing which is supported by the U.S. Department of Energy National Nuclear Security Administration under Contract No.

89233218CNA000001, and with the Extreme Science and Engineering Discovery Environment (XSEDE), which is supported by National Science Foundation (NSF) grant number ACI-1548562. YL and PK are grateful for insightful comments from Chengkun Huang.

## Appendix A. Asymptotic NCI growth rate

We can calculate the growth rate in Eq(7) in WT scheme by substituting Eq(10) and (11) into Eq(7). We calculate the common factor in  $S_{B3}\xi_0 - S_{E2}[k]_{B1}$

$$\frac{S_{B3}\xi_0 - S_{E2}[k]_{B1}}{s_{l-1,1}s_{l,2}\tau_{l,3}\eta_2} = \cos(\omega'\Delta t/2)\left(\frac{\sin(k'_1\Delta x_1/2)}{k'_1\Delta x_1/2}\right)(-1)^{\nu_1}\left(\frac{\sin(k'_1\Delta t/2)}{\Delta t/2}\right) - \left(\frac{\sin(k'_1\Delta t)}{k'_1\Delta t}\right)\left(\frac{\sin(k_1\Delta x_1/2)}{\Delta x_1/2}\right) \quad (\text{A.1})$$

Using the fact that the NCI resonance satisfies the dispersion relation of the beam  $\omega' = ck'_1$ , we have

$$\begin{aligned} \frac{S_{B3}\xi_0 - S_{E2}[k]_{B1}}{s_{l-1,1}s_{l,2}\tau_{l,3}\eta_2} &= \cos(k'_1c\Delta t/2)\left(\frac{\sin(k'_1\Delta x_1/2)}{k'_1\Delta x_1/2}\right)(-1)^{\nu_1}\left(\frac{\sin(k'_1\Delta t/2)}{\Delta t/2}\right) - \left(\frac{\sin(k'_1\Delta t)}{k'_1\Delta t}\right)\left(\frac{\sin(k_1\Delta x_1/2)}{\Delta x_1/2}\right) \\ &= \left(\frac{\sin(k'_1\Delta x_1/2)}{k'_1\Delta x_1/2}\right)(-1)^{\nu_1}\left(\frac{\sin(k'_1\Delta t)}{\Delta t}\right) - \left(\frac{\sin(k'_1\Delta t)}{k'_1\Delta t}\right)\left(\frac{\sin(k_1\Delta x_1/2)}{\Delta x_1/2}\right) \\ &= \frac{\sin(k'_1\Delta x_1/2)(-1)^{\nu_1} - \sin(k_1\Delta x_1/2)}{k'_1\Delta t\Delta x_1/2} \end{aligned}$$

using  $k'_1 = k_1 + \nu_1 \frac{2\pi}{\Delta x_1}$  we have  $\sin(k'_1\Delta x_1/2) \times (-1)^{\nu_1} = \sin(k_1\Delta x_1/2)$ , thus

$$S_{B3}\xi_0 - S_{E2}[k]_{B1} = 0 \quad (\text{A.2})$$

In the same way, we can derive that

$$S_{B2}\xi_0 - S_{E3}[k]_{B1} = 0 \quad (\text{A.3})$$

Thus the NCI growth rate in Eq(7) is zero for WT scheme. The above derivation is valid for arbitrary aliasing beam and arbitrary spatial derivative stencil in Faraday's equation, as long as the ultra-relativistic beam is moving along the axis of the grid, and the spatial derivative stencil in Ampere's equation is not modified from the standard Yee stencil.

## Appendix B. The self force

As long as one use a charge conserving deposition scheme for calculating current density, the following Gauss's equation is conserved[13]

$$\hat{D} \cdot \mathbf{E} = 4\pi\rho \quad (\text{B.1})$$

where the difference operator  $\hat{D}_1(X_{n_1, n_2, n_3}) = \frac{1}{\Delta x_1}(X_{n_1+\frac{1}{2}, n_2, n_3} - X_{n_1-\frac{1}{2}, n_2, n_3})$  and similarly for the remaining spatial coordinates. Eq(B.1) is conserved automatically, if it is fulfilled in the initial moment. Following Ref. [4], the approximate equations used to solve the grid-defined electric fields can be formally expressed in the form

$$\mathbf{E}(\mathbf{x}_g) = V_c \sum_{g'} \mathbf{G}(\mathbf{x}_g; \mathbf{x}_{g'})\rho(\mathbf{x}_{g'}) \quad (\text{B.2})$$

We assume that the components of the Green's function  $\mathbf{G}$  satisfies symmetry under the interchange of one coordinate

$$\begin{aligned} G_1(\mathbf{x}_g; \mathbf{x}_{g'}) &= -G_1(x_{g',1}, x_{g,2}, x_{g,3}; x_{g,1}, x_{g',2}, x_{g',3}) \\ G_2(\mathbf{x}_g; \mathbf{x}_{g'}) &= -G_2(x_{g,1}, x_{g',2}, x_{g,3}; x_{g',1}, x_{g,2}, x_{g',3}) \\ G_3(\mathbf{x}_g; \mathbf{x}_{g'}) &= -G_3(x_{g,1}, x_{g,2}, x_{g',3}; x_{g',1}, x_{g',2}, x_{g,3}) \end{aligned} \quad (\text{B.3})$$

The symmetry can be inherited from the symmetry in the boundary condition, e.g. periodic boundary condition in each direction. Using the form-factor in Eq(2) and the force interpolation in Eq(16), the self electric force in  $x_1$  direction for a particle of charge  $q$  at position  $\mathbf{x} = (x_1, x_2, x_3)$  gives

$$\begin{aligned} F_{\text{self},1}(\mathbf{x}) &= F_{\text{self},1}(x_1, x_2, x_3) \\ &= q^2 \sum_{g,g'} G_1(\mathbf{x}_g; \mathbf{x}_{g'}) W_l(x_1 - x_{g,1}) T_l(x_2 - x_{g,2}) T_l(x_3 - x_{g,3}) \\ &\quad \times W_l(x_1 - x_{g',1}) W_l(x_2 - x_{g',2}) W_l(x_3 - x_{g',3}) \end{aligned} \quad (\text{B.4})$$

Using Eq(B.3) and interchanging  $x_{g,1}$  and  $x_{g',1}$  we have  $F_{\text{self},1}(\mathbf{x}) = -F_{\text{self},1}(\mathbf{x})$ , thus  $F_{\text{self},1}(\mathbf{x}) = 0$ . Similarly  $F_{\text{self},1}(\mathbf{x}) = F_{\text{self},2}(\mathbf{x}) = 0$ . The analysis for self force here only applies to the electrostatic part of the field. In full electromagnetic PIC, a more comprehensive analysis for the self force is desirable.

## Appendix C. Dispersion error of the Maxwell solver

The dispersion relation of electromagnetic waves for the Maxwell solvers with modified spatial derivative in Faraday's equation is[11]

$$s_\omega^2 = s_1^2 A_1 + s_2^2 A_2 + s_3^2 A_3 \quad (\text{C.1})$$

with the abbreviations

$$s_\omega = \frac{\sin(\omega\Delta t/2)}{c\Delta t}, \quad s_i = \frac{\sin(k_i\Delta x_i/2)}{\Delta x_i}, \quad i = 1, 2, 3 \quad (\text{C.2})$$

$$\begin{aligned} A_1 &= 1 - 2\beta_{12}[1 - \cos(k_2\Delta x_2)] - 2\beta_{13}[1 - \cos(k_3\Delta x_3)] - 2\delta_1[1 - \cos(k_1\Delta x_1)] \\ A_2 &= 1 - 2\beta_{23}[1 - \cos(k_3\Delta x_3)] - 2\beta_{21}[1 - \cos(k_1\Delta x_1)] - 2\delta_2[1 - \cos(k_2\Delta x_2)] \\ A_3 &= 1 - 2\beta_{31}[1 - \cos(k_1\Delta x_1)] - 2\beta_{32}[1 - \cos(k_2\Delta x_2)] - 2\delta_3[1 - \cos(k_3\Delta x_3)] \end{aligned} \quad (\text{C.3})$$

where are  $\beta_{ij}$  and  $\delta_i$  are dimensionless tunable parameters and the six  $\beta$  coefficients depend on  $\hat{\beta}_i$  as following

$$\hat{\beta}_1 = \frac{\Delta x_2^2}{c^2\Delta t^2}\beta_{12} = \frac{\Delta x_3^2}{c^2\Delta t^2}\beta_{13}, \quad \hat{\beta}_2 = \frac{\Delta x_3^2}{c^2\Delta t^2}\beta_{23} = \frac{\Delta x_1^2}{c^2\Delta t^2}\beta_{21}, \quad \hat{\beta}_3 = \frac{\Delta x_1^2}{c^2\Delta t^2}\beta_{31} = \frac{\Delta x_2^2}{c^2\Delta t^2}\beta_{32} \quad (\text{C.4})$$

In a PIC simulation, if the characteristic wavelength  $\lambda$  or wavevector  $k = \frac{2\pi}{\lambda}$  satisfies  $k\Delta x = \frac{2\pi\Delta x}{\lambda} \ll 1$ , then the dispersion properties near  $k\Delta x = 0$  is much more important than the dispersion properties in the rest of the  $k$  space. An approach for minimizing the dispersion error[11] can be done in general cases, but we focus on reducing the dispersion error near  $k\Delta x = 0$ . We expand the phase velocity  $v_g = \omega/k$  to second order using the the spherical coordinates for the wave vectors  $(k_1, k_2, k_3) = (k \sin \theta \cos \phi, k \sin \theta \sin \phi, k \cos \theta)$

$$\begin{aligned} \frac{\omega}{ck} &= 1 + \left[ \frac{c^2\Delta t^2 - \Delta x_1^2(1 + 12\delta_1)}{24} \sin^4 \theta \cos^4 \phi + \frac{c^2\Delta t^2 - \Delta x_2(1 + 12\delta_2)}{24} \sin^4 \theta \sin^4 \phi \right. \\ &\quad + \frac{c^2\Delta t^2 - \Delta x_3^2(1 + 12\delta_3)}{24} \cos^4 \theta + \frac{c^2\Delta t^2(1 - 12\hat{\beta}_1)}{48} \sin^2 2\theta \sin^2 \phi \\ &\quad \left. + \frac{c^2\Delta t^2(1 - 12\hat{\beta}_2)}{48} \sin^2 2\theta \cos^2 \phi + \frac{c^2\Delta t^2(1 - 12\hat{\beta}_3)}{48} \sin^4 \theta \sin^2 2\phi \right] k^2 + O(k\Delta x)^4 \end{aligned} \quad (\text{C.5})$$

If we require that the second order term is zero, then we obtain

$$\begin{aligned} c^2\Delta t^2 - \Delta x_1^2(1 + 12\delta_1) &= 0 & 1 - 12\hat{\beta}_1 &= 0 \\ c^2\Delta t^2 - \Delta x_2^2(1 + 12\delta_2) &= 0 & 1 - 12\hat{\beta}_2 &= 0 \\ c^2\Delta t^2 - \Delta x_3^2(1 + 12\delta_3) &= 0 & 1 - 12\hat{\beta}_3 &= 0 \end{aligned} \quad (\text{C.6})$$

which implies

$$\hat{\beta}_i = \frac{1}{12}, \quad \delta_i = \frac{(c\Delta t/\Delta x_i)^2 - 1}{12}, \quad \text{and } \beta_{ij} = \frac{(c\Delta t/\Delta x_j)^2}{12} \quad (\text{C.7})$$

## Appendix D. loading particles with relativistic distributions

The method for loading particles with relativistic distributions from Ref [13] can be generalized to arbitrary drifting directions. For relativistic PIC simulations, one usually need to load the pseudo-particles with shifted-Maxwell distribution. The particles can be loaded in the center-of-mass (CM) frame  $S'$  where the distribution function is isotropic and transformed into the simulation frame  $S$ , assuming that  $S'$  is moving at velocity  $\vec{\beta}c = \vec{n}\beta c$  with  $\beta < 1$  w.r. to  $S$ , and  $\gamma = 1/\sqrt{1 - \beta^2}$ . The commonly used momentum distribution in  $S'$  frame is usually the Jüttner-Synga distribution, which represents the thermal equilibrium state with relativistic temperature  $T \gtrsim \frac{mc^2}{k_B}$

$$f'(\vec{p}')d^3\vec{p}' = \frac{N}{4\pi \frac{k_B T}{mc^2} (mc)^3 K_2(\frac{mc^2}{k_B T})} \exp\left(-\frac{\sqrt{m^2c^2 + p'^2}}{k_B T/c}\right) d^3\vec{p}' \quad (\text{D.1})$$

where  $\vec{p}'$  is the momentum of the particle,  $N$  is the number of particles,  $m$  is the mass of one particle, and  $K_2(x)$  is the modified Bessel function of the second kind. In low temperature limit  $\frac{k_B T}{mc^2} \rightarrow 0$ , the distribution recovers the Maxwell-Boltzmann distribution

$$f'(\vec{p}')d^3\vec{p}' = \frac{N'}{(2\pi mk_B T)^{3/2}} \exp\left(-\frac{p'^2}{2mk_B T}\right) d^3\vec{p}' \quad (\text{D.2})$$



The momentum distribution can be initialized in  $S'$  using the widely used Box-Muller algorithm[16] for non-relativistic Maxwell-Boltzmann distribution in Eq(D.2), or Sobol algorithm[17] for relativistic Jüttner-Syngé distribution function in Eq(D.1). The momentum  $\vec{p}'$  loaded in  $S'$  are transformed into momentum  $\vec{p}$  in  $S$  frame by the Lorentz transform

$$\vec{p} = [\vec{p}' - (\vec{p}' \cdot \vec{n})\vec{n}] + \gamma(\vec{p}' \cdot \vec{n} + \beta \frac{E'}{c})\vec{n} \quad (\text{D.3})$$

where  $E' = \sqrt{p'^2 c^2 + m^2 c^4}$  is the energy of the particle in  $S'$  frame. The momentum distribution function  $f(\vec{p})$  in  $S$  frame is related to  $f(\vec{p}')$  by

$$f(\vec{p})d^3\vec{p} = \frac{E}{E'}f(\vec{p}')d^3\vec{p}' = \gamma(1 + \beta c \frac{\vec{p}' \cdot \vec{n}}{E'})f(\vec{p}')d^3\vec{p}' \quad (\text{D.4})$$

For the volume transform part  $\gamma(1 + \beta c \frac{\vec{p}' \cdot \vec{n}}{E'})$ , Ref. [13] proposed to use the rejection method. Another random number  $X_1 \in [0, 1]$  is needed to do the rejection. If  $\frac{1}{2}(1 + \beta c \frac{\vec{p}' \cdot \vec{n}}{E'}) > X_1$ , then we need to reject the pseudo-particle. However, if the particle distribution in  $S'$  is symmetric about the  $\vec{n}$  direction, i.e.  $f'(\vec{p}') = f'(\vec{p}' - 2\vec{n} \cdot \vec{p}'\vec{n})$  and an isotropic distribution in Eq(D.1) or Eq(D.2) is a special case for symmetric distribution, then because  $\frac{1}{2}(1 + \beta c \frac{(\vec{p}' - 2\vec{n} \cdot \vec{p}'\vec{n}) \cdot \vec{n}}{E'}) = \frac{1}{2}(1 - \beta c \frac{\vec{p}' \cdot \vec{n}}{E'}) < 1 - X_1$ , we can flip the momentum  $\vec{p}' \rightarrow \vec{p}' - 2\vec{n} \cdot \vec{p}'\vec{n}$  instead of rejecting the pseudo-particle if  $\frac{1}{2}(1 + \beta c \frac{\vec{p}' \cdot \vec{n}}{E'}) > X_1$ . Then for the symmetric distribution about the  $\vec{n}$  direction, the acceptance efficiency is 100%.

## Appendix E. Scaling for ultra-relativistic PIC simulations

We show that the equations for ultra-relativistic PIC modeling can be written in the dimensionless form with proper normalization. The equations for relativistic PIC modeling are

$$\begin{aligned} m_s \frac{d\mathbf{u}_s}{dt} &= q_s(\mathbf{E} + \frac{\mathbf{v}_s}{c} \times \mathbf{B}) \\ \frac{d\mathbf{x}_s}{dt} &= \mathbf{v}_s \\ \frac{\partial \mathbf{E}}{\partial t} &= c\nabla \times \mathbf{B} - 4\pi\mathbf{J} \\ \frac{\partial \mathbf{B}}{\partial t} &= -c\nabla \times \mathbf{E} \\ \mathbf{J} &= \sum_s w_s q_s \mathbf{v}_s \end{aligned} \quad (\text{E.1})$$

where  $s$  stands for  $s$ -th pseudo-particle and  $w_s$  is the weight of  $s$ -th pseudo-particle. We define the normalization

$$\begin{aligned} t &= \omega_{pe}^{-1} \tilde{t} & \mathbf{x}_s &= (c/\omega_{pe})\tilde{\mathbf{x}} & \mathbf{u}_s &= \gamma_0 c \tilde{\mathbf{u}}_s & \mathbf{v}_s &= c \tilde{\mathbf{v}}_s \\ m_s &= m_e \tilde{m}_s & q_s &= e \tilde{q}_s & \tilde{w}_s &= n_e \tilde{w}_s & \mathbf{E} &= \sqrt{4\pi\gamma_0 n_e m_e c^2} \tilde{\mathbf{E}} & \mathbf{B} &= \sqrt{4\pi\gamma_0 n_e m_e c^2} \tilde{\mathbf{B}} \end{aligned} \quad (\text{E.2})$$

where  $\omega_{pe} = \sqrt{\frac{4\pi n_e e^2}{\gamma_0 m_e}}$ , then we obtain the dimensionless equations

$$\begin{aligned} \frac{d\tilde{\mathbf{u}}_s}{d\tilde{t}} &= \frac{\tilde{q}_s}{\tilde{m}_s} (\tilde{\mathbf{E}} + \tilde{\mathbf{v}}_s \times \tilde{\mathbf{B}}) \\ \frac{d\tilde{\mathbf{x}}_s}{d\tilde{t}} &= \frac{\mathbf{v}_s}{c} \\ \frac{\partial \tilde{\mathbf{E}}}{\partial \tilde{t}} &= \tilde{\nabla} \times \tilde{\mathbf{B}} - \sum_s \tilde{w}_s \tilde{q}_s \tilde{\mathbf{v}}_s \\ \frac{\partial \tilde{\mathbf{B}}}{\partial \tilde{t}} &= -\tilde{\nabla} \times \tilde{\mathbf{E}} \end{aligned} \quad (\text{E.3})$$

and

$$\tilde{\mathbf{v}} = \frac{1}{\sqrt{1 + 1/\tilde{u}^2 \gamma_0^2}} \frac{\tilde{\mathbf{u}}}{\tilde{u}} = (1 - \frac{1}{2\tilde{u}^2 \gamma_0^2} + O(\frac{1}{\tilde{u}^4 \gamma_0^4})) \frac{\tilde{\mathbf{u}}}{\tilde{u}} \quad (\text{E.4})$$

If  $\gamma_0 \gg 1$  and  $\tilde{u} \gtrsim 1$ , then we have

$$\tilde{\mathbf{v}} = \frac{\tilde{\mathbf{u}}}{\tilde{u}} + O(\frac{1}{\gamma_0^2}) \quad (\text{E.5})$$

The dimensionless equations Eq(E.3) and Eq(E.5) are independent of the typical Lorentz factor  $\gamma_0$  of the ultra-relativistic system. The scaling relations in Eq(E.2) can be used for Lorentz factor scaling of the relativistic PIC simulations, i.e. the simulation results obtained for one value of  $\gamma_0$  can be scaled to get the results for other values of  $\gamma_0$  as long as  $\gamma_0$  is large.

## References

### References

- [1] C. Birdsall, Particle-in-cell charged-particle simulations, plus monte carlo collisions with neutral atoms, PIC-MCC, IEEE Transactions on Plasma Science 19 (2) (1991) 65–85. doi:10.1109/27.106800.
- [2] K. Yee, Numerical solution of initial boundary value problems involving maxwell’s equations in isotropic media, IEEE Transactions on Antennas and Propagation 14 (3) (1966) 302–307. doi:10.1109/tap.1966.1138693.
- [3] T. Esirkepov, Exact charge conservation scheme for particle-in-cell simulation with an arbitrary form-factor, Computer Physics Communications 135 (2) (2001) 144–153. doi:10.1016/s0010-4655(00)00228-9.
- [4] R. W. Hockney, J. W. Eastwood, Computer simulation using particles, 1988.
- [5] B. B. Godfrey, Numerical cherenkov instabilities in electromagnetic particle codes, Journal of Computational Physics 15 (4) (1974) 504–521. doi:10.1016/0021-9991(74)90076-x.
- [6] C.-K. Huang, Y. Zeng, Y. Wang, M. Meyers, S. Yi, B. Albright, Finite grid instability and spectral fidelity of the electrostatic particle-in-cell algorithm, Computer Physics Communications 207 (2016) 123–135. doi:10.1016/j.cpc.2016.05.021.
- [7] X. Xu, P. Yu, S. F. Martins, F. S. Tsung, V. K. Decyk, J. Vieira, R. A. Fonseca, W. Lu, L. O. Silva, W. B. Mori, Numerical instability due to relativistic plasma drift in EM-PIC simulations, Computer Physics Communications 184 (11) (2013) 2503–2514. doi:10.1016/j.cpc.2013.07.003.
- [8] J.-L. Vay, C. Geddes, E. Cormier-Michel, D. Grote, Numerical methods for instability mitigation in the modeling of laser wakefield accelerators in a lorentz-boosted frame, Journal of Computational Physics 230 (15) (2011) 5908–5929. doi:10.1016/j.jcp.2011.04.003.
- [9] I. V. Sokolov, Alternating-order interpolation in a charge-conserving scheme for particle-in-cell simulations, Computer Physics Communications 184 (2) (2013) 320–328. doi:10.1016/j.cpc.2012.09.015.
- [10] J. Brackbill, On energy and momentum conservation in particle-in-cell plasma simulation, Journal of Computational Physics 317 (2016) 405–427. doi:10.1016/j.jcp.2016.04.050.
- [11] A. Blinne, D. Schinkel, S. Kuschel, N. Elkina, S. G. Rykovanov, M. Zepf, A systematic approach to numerical dispersion in maxwell solvers, Computer Physics Communications 224 (2018) 273–281. doi:10.1016/j.cpc.2017.10.010.
- [12] B. B. Godfrey, J.-L. Vay, Improved numerical cherenkov instability suppression in the generalized PSTD PIC algorithm, Computer Physics Communications 196 (2015) 221–225. doi:10.1016/j.cpc.2015.06.008.
- [13] S. Zenitani, Loading relativistic maxwell distributions in particle simulations, Physics of Plasmas 22 (4) (2015) 042116. doi:10.1063/1.4919383.
- [14] L. Sironi, A. Spitkovsky, J. Arons, THE MAXIMUM ENERGY OF ACCELERATED PARTICLES IN RELATIVISTIC COLLISIONLESS SHOCKS, The Astrophysical Journal 771 (1) (2013) 54. doi:10.1088/0004-637x/771/1/54.
- [15] T. D. Arber, K. Bennett, C. S. Brady, A. Lawrence-Douglas, M. G. Ramsay, N. J. Sircombe, P. Gillies, R. G. Evans, H. Schmitz, A. R. Bell, C. P. Ridgers, Contemporary particle-in-cell approach to laser-plasma modelling, Plasma Physics and Controlled Fusion 57 (11) (2015) 113001. doi:10.1088/0741-3335/57/11/113001.
- [16] G. E. P. Box, M. E. Muller, A note on the generation of random normal deviates, The Annals of Mathematical Statistics 29 (2) (1958) 610–611. doi:10.1214/aoms/1177706645.
- [17] I. Sobol, On modeling certain distributions similar to gamma distribution, Monte Carlo Methods in Computational Mathematics and Mathematical Physics (1976) 24–29.